İSTANBUL UNIVERSITY CERRAHPAŞA

ORIGINAL ARTICLE
Electrica 2024; 24(2): 385-391

Electrostatic Discharge Cross Talk Attenuation in Protective Meander Lines

Georgiy Y. Kim, Alexander V. Nosov

Department of Television and Control, Tomsk University of Control Systems and Radioelectronics, Tomsk, Russian Federation

Cite this article as: G. Y. Kim and A. V. Nosov, "Electrostatic discharge cross talk attenuation in protective meander lines," *Electrica*, 24(2), 385-391, 2024.

ABSTRACT

It is known that electrostatic discharge (ESD) is one of the frequent causes of integrated circuit failure and loss of spacecraft. However, the danger is not only the pulse itself but also the cross talk from it at the near (NEXT) and far (FEXT) ends. To investigate the possibility of their attenuating by meander line (ML) with a broadside coupling, a coupled microstrip line (MSL) was studied. As a result, the structure with a protected active line appeared to be the most promising. Also, the levels of NEXT and FEXT in it do not exceed 2% and 1.5% of half of the e.m.f. at $s = 1000$ μm, and when $s = 100$ μm 10% and 3%. In addition to evaluating signal attenuation, N-norms were analyzed as well. The most noteworthy is the nonlinear nature of the change in $N2$ depending on s. It is also notable that the proposed protection of the line from cross talk leads to a decrease in $N1$, $N2$, and $N5$. However, $N3$ and $N4$ increase at the same time.

***Index Terms*—**Coupled lines, cross talk, electrostatic discharge, meander line, protective device

I. INTRODUCTION

Ensuring electromagnetic compatibility (EMC) is an important stage in the design of modern radio-electronic equipment (REE). One of the purposes of the EMC is protection against conductive electromagnetic interference (EMI) penetrating the REE directly through the conductors [1]. Among this interference, electrostatic discharge (ESD) should be singled out, which under certain conditions can become conducted interference. The main sources of ESD accumulation and transfer are humans, charged dielectrics, and insulated metal parts. Currently, three main forms of current have been standardized to study the immunity to the ESD impact: a human body model (HBM) [2], a mechanical model [3], and a model of a charged device [4]. In addition, other models describing ESD current forms are being developed, for example, a model of a charged printed circuit board [5] and a model of a charged cable [6–8]. There are many circuit engineering models that implement the forms of the ESD current pulses. These models allow calculating currents and voltages in the REE circuit analysis [9–16]. In general, ESD can lead to partial or complete failure of REE, as well as to the interruption of its functioning. Therefore, it is necessary to apply effective measures that protect REE against ESD. However, despite the danger of ESD, it is not always possible to provide effective protection against it [17-19]. Thus, ESD is known to be one of the frequent causes of failure and loss of spacecraft [20]. It is also known that the probability of failure of integrated circuits (IC) that are in contact with an ESD source is about 0.619 [21]. This high value indicates a low resistance of the IC to the destructive effects of external discharges. The danger of ESD exposure on REE is worsened by the fact that traditional protection devices have a number of shortcomings [1], in particular, insufficient speed and low power. Therefore, it is necessary to search and investigate new protection devices that are devoid of imperfections of traditional ones.

One such solution is a device based on adaptive dielectric thin-film transistors [22]. Their advantage is the possibility of ESD shunting at low leakage currents during normal operation. Another solution is to use materials that can transition from a non-conducting state to a conducting one. For example, a switch based on vanadium dioxide can provide bidirectional ESD protection with an amplitude from 1 to 15 kV [23]. Yet another solution is an approach based on the decomposition of an interference pulse into a sequence of pulses of smaller amplitudes, known as modal

Corresponding author:
Georgiy Y. Kim

E-mail:
kimgeoju@gmail.com

Received: December 05, 2023

Revision Requested: January 22, 2024

Last Revision Received: February 25, 2024

Accepted: February 25, 2024

Publication Date: April 17, 2024

DOI: 10.5152/electrica.2024.23178

filtering [24]. This approach may not require a dedicated protection device but relies on the conductors available on the printed circuit boards. Devices using this approach are called modal filters (MF). Similar to MFs are protective meander lines (MLs) [25]. The use of ML for interference decomposition has a number of advantages over MFs: a 2× shorter structure length, a larger number of decomposition pulses due to the presence of cross talk (when comparing the cross sections of two-conductor MLs and MFs), the possibility of the absence of a dielectric. It is also important to mention the study of the decomposition of the ESD peak emission by HBM in the meander MSL [26]. Due to this decomposition, its attenuation was up to 1.44, 1.3, and 4.6 times at distances between conductors (*s*) of 50, 150, and 1 µm, respectively. Thus, to ensure maximum ESD attenuation in a meander MSL, a strong coupling between the conductors is required. This coupling in the structure of a meander MSL is achieved because of a small *s*. However, this also makes it difficult to implement such a device in practice. Therefore, a more promising structure has been investigated, an ML with a broadside coupling [27], which allows the ESD attenuation of up to 1.61 times. In such a structure, the coupling between the conductors depends on the thickness of the dielectric substrate.

In addition, when analyzing the ESD impact on signal conductors, it is also important to measure its cross talk on passive conductors. Thus, a number of studies have estimated the influence of grounding methods and the width of the protective path in coupled lines on the amplitude of cross talk [28, 29]. It was revealed that an increase in the width of the protective path by two and three times can lead to a decrease in the amplitude of the cross talk by 1.2 and 1.5 times. Moreover, the cross talk at the far end can be reduced by 1.5 times with a certain connection of the protective path. Reducing cross talk is an urgent task of REE EMC. Therefore, the purpose of this work is to investigate the possibility of reducing cross talk from ESD using an ML with broadside coupling.

II. INITIAL DATA

For this study, we chose an MSL consisting of active and passive conductors that are located parallel to each other and connected to a path with *Z*=50 Ω. The cross section and circuit diagram of this MSL are shown in Fig. 1 (hereinafter, for simplicity, we will call it structure 1). Here and further on the circuit diagrams, we mark only the nodes in which the response will be calculated. The cross-sectional parameters were chosen so that $(Z_e Z_o)^{0,5}$ = 50 Ω: the width and thickness of the conductors *w* = 726 µm and *t* = 18 µm, the thickness of the substrate *h* = 500 µm, and the dielectric constant of the substrate

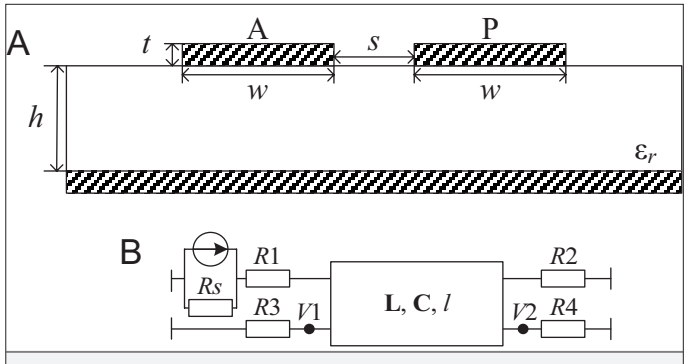

Fig. 1. Cross section (a) and circuit diagram (b) of the MSL.

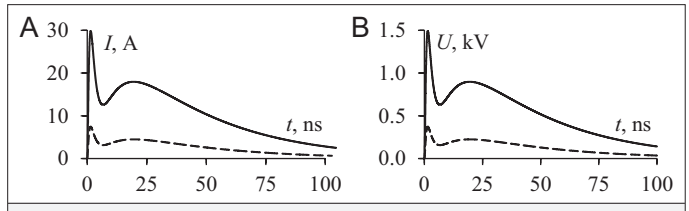

Fig. 2. Waveforms of ESD currents (a) and voltages (b) of I (– –) and IV (––) test levels according to IEC 61000-4-2.

ε_r = 4.5. The length of the line was *l*=100 mm. Resistances on the diagram were *R*1 = *R*2 = *R*3 = *R*4 = 50 Ω. The ESD source is presented by a current source connected in parallel with a resistor *Rs* = 1 MΩ. As an excitation, we took the ESD form according to the HBM, corresponding to the I and IV degrees of hardness, according to IEC 61000-4-2 [30]. Further, for simplicity, we will call them ESD 1 and ESD 4. Their current and voltage waveforms are shown in Fig. 2. Note that further evaluation will be performed on the example of the ESD voltage form.

III. MAIN RESULTS

First, we evaluated the effect of *s* on the amplitude of cross talk from ESD at the near (NEXT) and far (FEXT) ends at nodes *V*1 and *V*2 in Fig. 1, respectively. Fig. 3 shows the responses in node *V*1 and Fig. 4—in node *V*2 at *s* = 100, 550, and 1000 µm, obtained in Keysight advanced design system (ADS) and analytically [31] under the excitation from Fig. 2.

Figs. 3 and 4 demonstrate that the simulation results almost completely match the analytical calculations. The maximum root-mean-square error is 17% (Fig. 4B). With ESD 4, the maximum amplitudes of NEXT and FEXT were 249.62 and 68.13 V, 86.20 and 49.75 V, and 45.19 and 36.18 V for *s* = 100, 550, 1000 µm, respectively. With ESD 1, they were 62.40 and 17.03 V, 21.55 and 12.44 V, and 11.30 and 9.04

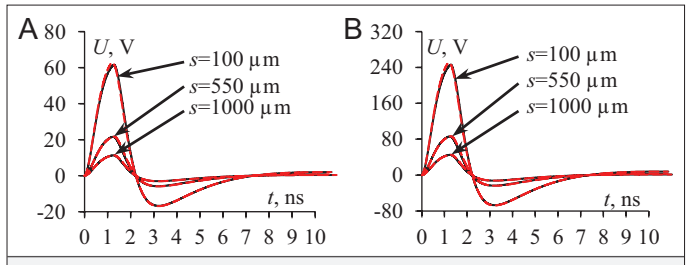

Fig. 3. Modeled (––) and analytically calculated (– –) NEXT for ESD 1 (a) and ESD 4 (b).

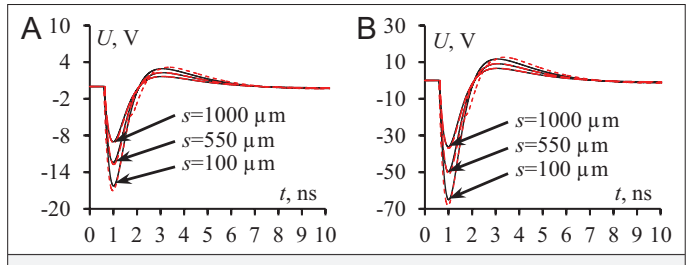

Fig. 4. Modeled (––) and analytically calculated (– –) FEXT for ESD 1 (a) and ESD 4 (b).

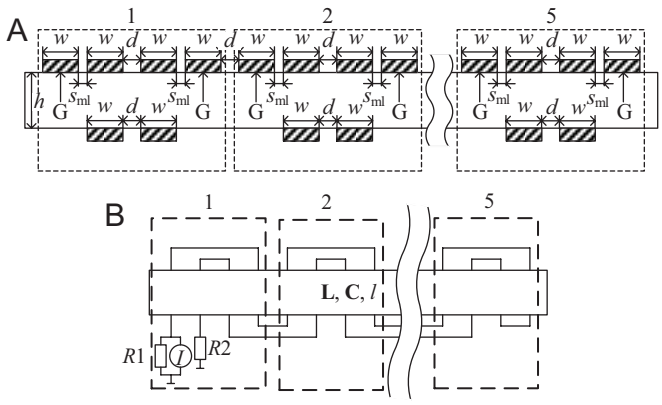

Fig. 5. Cross section (a) and circuit diagram (b) of the protective ML with broadside coupling.

V for s = 100, 550, and 1000 μm, respectively. The amplitudes of the cross talk from the signals in Fig. 2B, for NEXT and FEXT, are 16.73% and 4.57%, 5.78% and 3.33%, and 3.03% and 2.42% for s = 100, 550, and 1000 μm, respectively.

Second, we considered the possibility of reducing cross talk by using a protective ML with broadside coupling. For this purpose, a model of the ML with broadside coupling was created based on its *S*-parameters measured experimentally [27]. Fig. 5 shows a cross section and connection diagram of a protective ML with a broadside coupling.

Prior to experimental measurements, the topology of the ML layout with broadside coupling was developed using the following parameters obtained in the optimization phase: w=7.5 mm, t=18 μm, d=3w, s_{ml}=5.5 mm, h=1.5 mm and ε_r=4. We used SMA connectors manufactured by Molex with an operating frequency of 18 GHz and a wave impedance of 50 Ohms. The printed circuit board (PCB) with the ML layout was manufactured by "Elektrokonnect" Ltd. in Novosibirsk. Fig. 6 shows the PCB with the ML layout with broadside coupling.

Note that the PCB with ML and a broadside coupling layout in Fig. 6 is designed to operate in DC circuits with a current of 2.31 A and a voltage of 1.1 kV. Therefore, its dimensions can be significantly reduced for operation in lower current and voltage, AC, or signal circuits. This

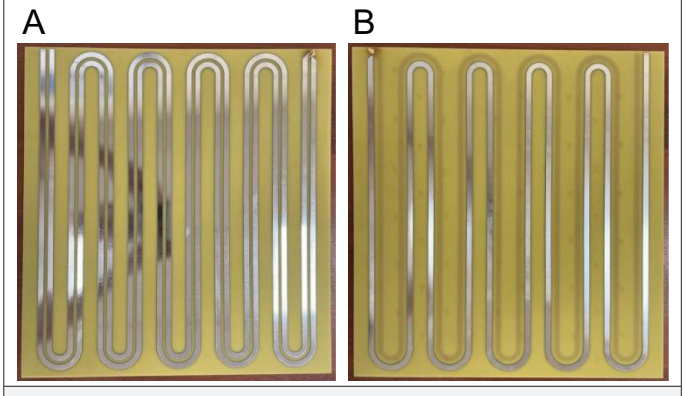

Fig. 6. PCB with ML with a broad-side coupling layout: top view (a) and bottom view (b).

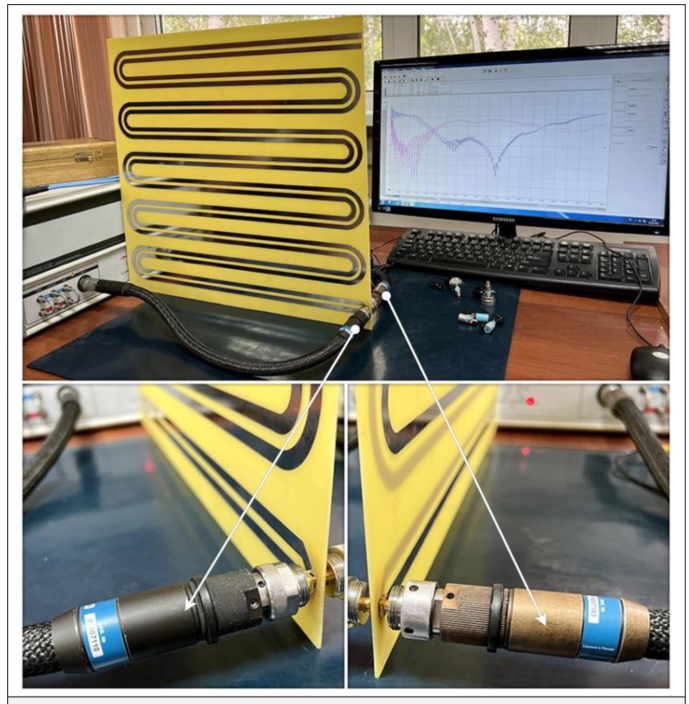

Fig. 7. Experimental setup for analyzing the frequency response of an ML turn with a broadside coupling.

can be achieved by optimizing the geometric parameters according to the relevant criteria while maintaining the protective properties. After the PCB with the ML layout was manufactured, its *S*-parameters were measured using the R4M-18 vector circuit analyzer manufactured by "Mikran" JSC. For this purpose, the PCB with the ML layout was connected to the analyzer using ultra-high frequency phase-stable cables. The frequency response was analyzed in the range from 10 MHz to 5 GHz. A two-port SOLT calibration was performed prior to the measurements. The experimental setup for the frequency response analysis is shown in Fig. 7

Two configurations were studied: with the ML at the input of the active conductor of the MSL and with the ML at both ends of its passive conductor (hereinafter, for simplicity, we will call them structures 2 and 3, respectively). The measurements were made when the lines were matched, at s = 1000 μm and s = 100 μm, and with the second excitation from Fig. 2. Fig. 8 shows the circuit diagrams of structures

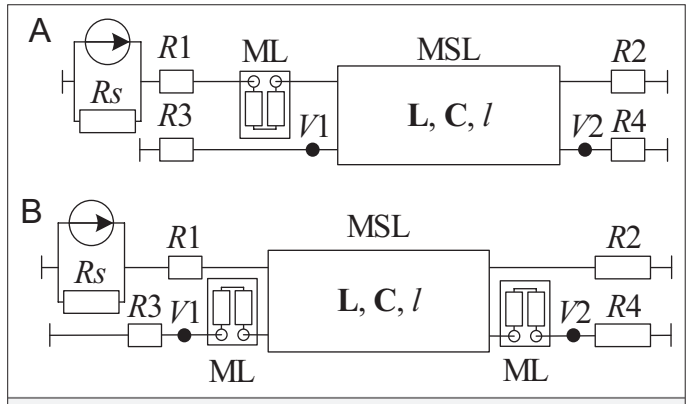

Fig. 8. Circuit diagrams of structures 2 (a) and 3 (b).

2 and 3, where ML is the ML with broadside coupling (Fig. 5) with *S*-parameters measured on the experimental setup from Fig. 7 The MSL cross sections in structures 2 and 3 are the same as in Fig. 1A, and the ML cross sections are the same as in Fig. 5A.

Comparison of the obtained time responses in nodes *V*1 and *V*2 of the MSL without the ML and with it is shown in Fig. 9. They were calculated in ADS based on the experimentally measured *S*-parameters of the ML with a broad-side coupling (setup in Fig.**7**) and the MSL model built in ADS.

Figs. 9 and 10 show that in structure 2, the maximum amplitudes of NEXT and FEXT do not exceed 29.67 and 23.35 V when s = 1000 μm and 163.45 and 43.94 V when s = 100 μm, respectively. In structure 3, these values are 28.1 and 21.75 V, and 155.53 and 39.64 V, respectively. Thus, in structure 2, NEXT and FEXT were reduced by 34% and 36% when s = 100 and 1000 μm, respectively, and in structure 3 by 38% and 40% when s = 100 and 1000 μm. Since structure 2 is simpler than structure 3, it is the most promising for practical application. Moreover, the active line is additionally protected in structure 2 [27].

A high voltage amplitude of the ESD can lead to an electrical breakdown, a fast rise time—to sparking, the average effective voltage value—to component burnout, etc. Therefore, as a third step, we evaluated the probability of occurrence of these factors by analyzing the *N*-norms of structures 1–3 [32]. Table I shows the names, equations, and applications of each norm.

Since the character of changes in *N*-norms will be the same for both effects from Fig. 2, they were calculated only for ESD 4. Figs. 11, 12, and 13 show the calculated *N*-norms in nodes *V*1 and *V*2 of all three structures with a change in s in the range of 50–1000 μm with a step of 50 μm.

In Fig. 11 for structure 1, it can be seen that increasing s reduces the values of all norms in node *V*1, which reduces the risks associated

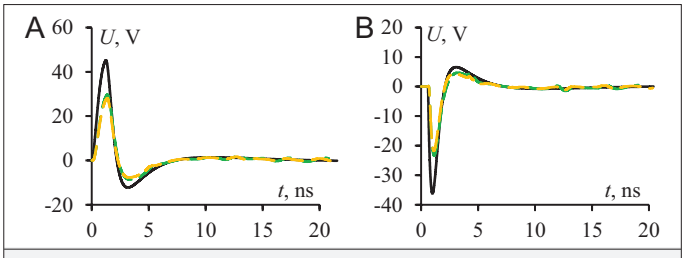

Fig. 9. NEXT (a) and FEXT (b) of structures 1 (––), 2 (– –), and 3 (– –) for s = 1000 μm.

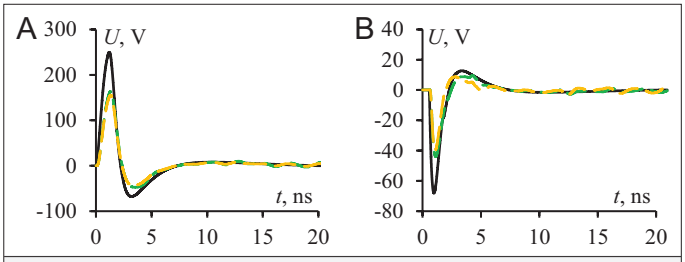

Fig. 10. NEXT (a) and FEXT (b) of structures 1 (––), 2 (– –), and 3 (– –) for s = 100 μm.

TABLE I. *N*-NORMS DESCRIPTIONS AND APPLICATIONS

Norm Equation	Name	Application
$N1 = \lvert R(t)\rvert_{max}$	Peak (absolute) value	Circuit upset/electric breakdown/arc-over effects
$N2 = \left\lvert \frac{\partial R(t)}{\partial t} \right\rvert_{max}$	Peak (absolute) derivative	Component arcing / circuit upset
$N3 = \left\lvert \int_0^t R(t)dt \right\rvert_{max}$	Peak (absolute) impulse	Dielectric puncture (if R denotes E field)
$N4 = \int_0^\infty \lvert R(t)\rvert dt$	Rectified total impulse	Equipment damage
$N5 = \left\{ \int_0^\infty \lvert R(t)\rvert^2 dt \right\}^{\frac{1}{2}}$	Square root of action integral	Component burnout

with them. In the *V*2 node, the norms increase with increasing s up to 150 μm and then decrease monotonously. It is important to note that N2 has a stepped character.

When s = 1000 μm in nodes *V*1 and *V*2 of structure 1, the norms decreased (relative to the norms of structure 1 when s = 50 μm) by the following values: *N*1—83% and 38%, *N*2—81% and 39%, *N*3—84% and 5%, *N*4—83% and 15%, *N*5—83% and 29%, respectively.

Figs. 12 and 13 show that the nature of changes in norms with an increase in s is similar to Fig. 11. When s = 1000 μm in nodes *V*1 and

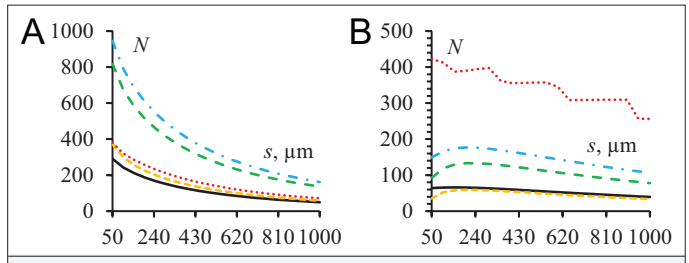

Fig. 11. Relationship between *N*1 (––), *N*2·10^{-9} (· · ·), *N*3·10^{10} (- - -), *N*4·10^{9} (– –), and *N*5·10^{5} (– · –) and s in nodes *V*1 (a) and *V*2 (b) for structure 1.

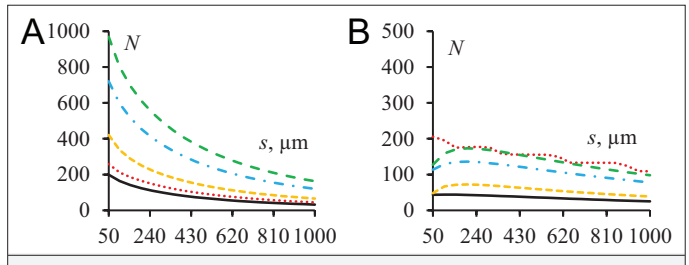

Fig. 12. Relationship between *N*1 (––), *N*2·10^{-9} (· · ·), *N*3·10^{10} (- - -), *N*4·10^{9} (– –), and *N*5·10^{5} (– · –) and s in nodes *V*1 (*a*) and *V*2 (*b*) for structure 2.

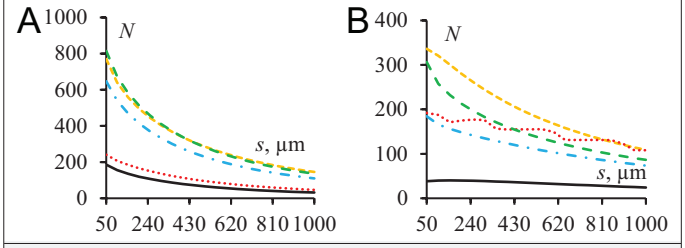

Fig. 13. Relationship between *N*1 (––), *N*2·10^{-9} (· · ·), *N*3·10^{10} (- - -), *N*4·10^{9} (– –), and *N*5·10^{5} (– · –) and *s* in nodes *V*1 (a) and *V*2 (b) for structure 3.

*V*2 of structure 2, the norms decreased (relative to the norms of structure 2 when $s = 50$ μm) as follows: *N*1 by 84% and 42%, *N*2 by 83% and 47%, *N*3 by 84% and 20%, *N*4 by 83% and 23%, and *N*5 by 83% and 31%, respectively. Similarly, in structure 3, the decreases were as follows: *N*1 by 83% and 37%, *N*2 by 81% and 44%, *N*3 by 81% and 68%, *N*4 by 83% and 72%, and *N*5 by 83% and 60%, respectively.

For clarity, Table II summarizes the average values of the norms for all the considered cases and their changes (Δ) relative to the case in Fig. 1 (where the signs "–" and "+" mean a decrease and an increase, respectively).

Table II shows that *N*1, *N*2, and *N*5 in structures 2 and 3 decreased, and the maximum difference between the average values of these norms was 7%. Meanwhile, *N*3 and *N*4 increased in both structures. Thus, an increase in these norms in nodes *V*1 and *V*2 of structure 2 is no more than 19% and 28%, and in structure 3 127% and 325%, respectively. Therefore, structure 2 is the most effective for suppressing ESD cross talk.

IV. CONCLUSIONS

The study demonstrated the possibility of attenuating NEXT and FEXT in a coupled MSL. Additionally, the cross talk was estimated in this structure by means of quasi-static modeling and analytical calculations. The study also demonstrated that NEXT and FEXT can be attenuated using a protective ML with broadside coupling. In this case, the level of NEXT and FEXT does not exceed 2% and 1.5% of half of the e.m.f. when $s = 1000$ μm, and 10% and 3% when $s = 100$ μm, respectively. The maximum NEXT and FEXT attenuations were 1.6 and 1.7 times, respectively.

According to the IEC 61000-4-25 [33] standard, the attenuation of cross talk should be at least 20 dB. In this study, its level is not more than 10% of the voltage in Fig. 2B. In the line with $s = 1000$ μm, even without protection, the level of cross talk does not exceed 3% of half of the e.m.f. However, when $s = 100$ μm, NEXT is 16.73% of half of the e.m.f. level in a two-wire MSL without a protective ML, and when using a protective ML 10%. As a result, the ML with a broadside coupling can be used both to protect against dangerous conducted interference and to protect against high levels of cross talk. This is especially important considering the trends toward the miniaturization of printed circuit boards and an increase in the density of components on them. For example, the use of the proposed method of protection will completely eliminate the threat of cross talk from ESD 1 in the CAN bus for chips manufactured by Texas Instruments HVDA55x-Q1 series [34], as well as significantly reduce the risk of damage to this component because of ESD 4. In addition, the proposed device will also weaken the voltage of the ESD when it passes through the active conductor.

TABLE II. AVERAGE *N*-NORMS COMPARISON

			***V*1**		
Structure	***N*1 (Δ1)**	***N*2 (Δ2)**	***N*3 (Δ3)**	***N*4 (Δ4)**	***N*5 (Δ5)**
1	120	167	145	332	392
2	80 (–34%)	107 (–36%)	163 (+12%)	397 (+19%)	294 (–25%)
3	77 (–36%)	108 (–35%)	329 (+127%)	332 (0%)	268 (–32%)
			***V*2**		
Structure	***N*1 (Δ1)**	***N*2 (Δ2)**	***N*3 (Δ3)**	***N*4 (Δ4)**	***N*5 (Δ5)**
1	55	345	47	108	147
2	35 (–35%)	152 (–56%)	56 (+20%)	139 (+28%)	110 (–25%)
3	33 (–39%)	150 (–57%)	199 (+325%)	155 (+43%)	115 (–21%)

Peer-review: Externally peer-reviewed.

Author Contributions: Concept – G.K., A.N.; Design – G.K., A.N.; Supervision – A.N.; Resources – G.K.; Materials – G.K.; Data Collection and/or Processing – G.K.; Analysis and/or Interpretation – G.K.; Literature Search – G.K., A.N.; Writing – G.K.; Critical Review – A.N.

Declaration of Interests: The authors have no conflicts of interest to declare.

Funding: The research was supported by the Ministry of Science and Higher Education of the Russian Federation (Project No: FEWM-2024-0005).

REFERENCES

1. Z. M. Gizatullin, and R. M. Gizatullin, "Investigation of the immunity of computer equipment to the power-line electromagnetic interference," *J. Commun. Technol. Electron.*, vol. 61, no. 5, pp. 546–550, 2016. [CrossRef]
2. GOST R 53734.3.1-2013. Elektrostatika. Metody modelirovaniya elektrostaticheskih yavlenij. Elektrostaticheskij razryad. Model' chelovecheskogo tela.– M.: Standartinform, 2014. – 11 p. (in Russian)
3. GOST R 53734.3.2-2013 (MEK 61340-3-2:2006). Elektrostatika. Metody modelirovaniya elektrostaticheskih yavlenij. Elektrostaticheskij razryad. Model' mekhanicheskogo ustrojstva. – M.: Standartinform, 2013. – 11 p. (in Russian).
4. GOST R 53734.3.3-2016. Metody modelirovaniya elektrostaticheskih yavlenij. Elektrostaticheskij razryad. Model' zaryazhennogo ustrojstva. – M.: Standartinform, 2016. – 23 p. (in Russian).
5. Industry Council on ESD Target Levels. White paper 2: A case for lowering component level CDM ESD specifications and requirements, industry council on ESD target levels. Revision 2.0, 2010. – 173 p.
6. W. Stadler, T. Brodbeck, R. Gaertner, and H. Gossner, Cable discharges into communication interfaces. Proceedings of the EOS/ESD Symposium, Tucson, AZ, USA, 2006, pp. 144–151.
7. K. Chatty, *Model-Based Guidelines to Suppress Cable Discharge Event (CDE) Induced Latch up in CMOSICs*. Proc. IEEE Int. rel. phys. symp. – Phoenix. AZ, USA, 2004, pp. 130–134.
8. C. J. Brennan, K. Chatty, J. Sloan, P. Dunn, M. Muhammad, and R. Gauthier, *Design Automation to Suppress Cable Discharge Event (CDE) Induced Latch up in 90-nm CMOSASICs*. Proc. EOS/ESD symp. – Anaheim. CA, USA, 2005, pp. 126–130.
9. S. Caniggia, and F. Maradei, "Circuit and numerical modeling of electrostatic discharge generators," *IEEE Trans. Ind. Appl.*, vol. 42, no. 6, pp. 1350–1357, 2006. [CrossRef]

10. T. Takada, T. Sekine, and H. Asai, *Circuit/Electromagnetic Hybrid Simulation of Electrostatic Discharge in Contact Discharge Mode*. Proc. Int. symp. electromagn. compat. – Rome, Italy, 2012, pp. 1–6. [CrossRef]
11. T. Yoshida, and N. Masui, *A Study on System Level ESD Stress Simulation Using Circuit Simulator*. Proc. Asia-Pacific symp. electromagn. compat. – Melbourne. Australia, 2013, pp. 1–4. [CrossRef]
12. Y. Zhou, and J. J. Hajjar, *A Circuit Model of Electrostatic Discharge Generators for ESD and EMC Spice Simulation*. Chengdu, China, 2014, pp. 1–2. [CrossRef]
13. K. Wang, D. Pommerenke, R. Chundru, T. V. Doren, J. L. Drewniak, and A. Shashindranath, "*Numerical modeling of electrostatic discharge generators. IEEE" Trans. on electromag. Comp*, vol. 45, no. 2, pp. 258–271, 2003.
14. J. Yousaf, M. Park, H. Lee, J. Youn, D. Lee, C. Hwang, "Efficient circuit and an EM model of an electrostatic discharge generator," *IEEE Trans. Electromagn. Compat.*, vol. 60, no. 4, pp. 1078–1086, 2018. [CrossRef]
15. H.-N. Lin, B.-N. Ko, J. Y. Lin, T.-H. Ho, M. Lin, and C. Su, Establishment of ESD generator model for transient susceptibility analysis from chip to system level. Joint Int. symp. on electromag. comp. – Sapporo, Japan, 2019, pp. 209–212. [CrossRef]
16. Y. Xiu, N. Thomson, R. Mertens, and E. Rosenbaum, S-parameter based modeling of system-level ESD test bed. 37th electrical overstress/elec trostatic discharge symposium (EOS/ESD). Reno, 2015, 2015, pp. 1–10.
17. C. Baum, W. Baker, W. Prather, J. Lehr, J. O. Loughlin, D. Giri, et al. JOLT: a highly directive, very intensive, impulse-like radiator. *Proceedings of the IEEE*. 2004, vol. 92, pp. 1096–1109.
18. M. Armanious, J. S. Tyo, M. C. Skipper, M. D. Abdalla, W. D. Prather, and J. E. Lawrance, "Interaction between geometric parameters and output waveforms in high-power quarterwave oscillators," *I.E.E.E Trans. Plasma Sci.*, vol. 38, no. 5, pp. 1124–1131, 2010. [CrossRef]
19. M. Backstrom, "Lovstrand," *Susceptibility of Electronic Systems to High-Power Microwaves: Summary of Test Experience, IEEE Transactions on. Electromagnetic Compatibility*, Vol. 46, 2004, pp. 396–403.
20. A. B. Sokolov, *Obespechenie Stojkosti Bortovoj Radioelektronnoj Apparatury Kosmicheskih Apparatov k Vozdejstviyu Elektrostaticheskih Razryadov. Dis. Dokt, tekhn. Nauk*. Moscow: Moscow State Institute of Electronics and Mathematics, 238pp. (in Russian), 2009. [*Ensuring the Stability of Onboard Radio-Electronic Equipment of Space Vehicles to the Influence of Electrostatic Discharges, Extended Admin. of* D.Sc. Thesis].
21. O. E. Malinova, and V. V. Zhadnov, *Issledovanie Matematicheskih Modelej Stojkosti IS k Vozdejstviyu ESR [Study of Mathematical Models of IC Resistance to ESD]. Sbornik Nauchnyh Trudov Vserossijskoj Nauchno-Tekhnicheskoj Konferencii Molodyh Uchenyh I Studentov, Posvyashchennoj*, Vol. 121-j godovshchine Dnya radio [Proceedings of the All-Russian Scientific and Technical Conference of Young Scientists and Students, dedicated to the 121st anniversary of Radio Day]. Krasnoyarsk, 2016, pp. 454–458. (in Russian).
22. P. Bhattacharya, R. Sinha, B. K. Thakur, V. Parab, M. Shrivastava, and S. Sambandan, "Adaptive dielectric thin film transistors-A self-configuring device for low power electrostatic discharge protection," *IEEE Electron Dev. Lett.*, vol. 41, no. 1, pp. 66–69, 2020. [CrossRef]
23. S. M. Bohaichuk, M. M. Pelella, Y. Sun, Z. Zhang, S. Ramanathan, and E. Pop, "VO_2 switch for electrostatic discharge protection," *IEEE Electron Dev. Lett.*, vol. 41, no. 2, pp. 292–295, 2020. [CrossRef]
24. A. M. Zabolotsky, and T. R. Gazizov, *Modal'nye fil'try Dlya Zashchity Bortovoj Radioelektronnoj Apparatury Kosmicheskogo Apparata* [*Modal Filters for the Protection of Onboard Electronic Equipment of a Spacecraft*]. Tomsk: Tomsk State University of Control Systems and Radioelectronics Publishing, 2013, 151pp. (in Russian).
25. R. S. Surovtsev, and A. V. Nosov, *Modal'noe Razlozhenie V Meandrovyh Liniyah I Ustrojstvah na Ih Osnove. Monografiya [Modal Decomposition in Meander Lines and Devices Based on Them]*. Tomsk: Tomsk State University of Control Systems and Radioelectronics Publishing, 2022, 184pp. (in Russian).
26. R. S. Surovtsev, A. V. Nosov, and T. R. Gazizov, "Using a turn of a meander microstrip line for ESD protection," *Electrica*, vol. 22, no. 1, pp. 84–91, 2022. [CrossRef]
27. A. V. Nosov, "Oslablenie vliyaniya elektrostaticheskogo razryada vitkom meandrovoj linii s licevoj svyaz'yu," *Sistem. Upravleniya Svyazi Bezopasnosti*, vol. 2, pp. 1–22, 2023. (in Russian).
28. I. A. Skornyakov, "Ocenka vliyaniya sposobov zazemleniya zashchitnoj trassy svyazannoj dvuhprovodnoj linii na perekrestnye navodki," *Sb. Izbrannyh Statej Nauchnoj Sessii TUSUR*, vol. 1–2, pp. 83–86, 2021. (in Russian).
29. I. A. Skornyakov, and R. S. Surovcev, "Analiz vliyaniya shiriny razvyazyvayushchej trassy na amplitudu perekrestnyh navodok v svyazannoj dvuhprovodnoj linii," *Sb. Izbrannyh Statej Nauchnoj Sessii TUSUR*, vol. 1–2, pp.86–91, 2021. (in Russian).
30. *IEC 61000-4-2 (2008), Electromagnetic Compatibility (EMC) Part 4: Testing and Measurement Techniques – Section 2: Electrostatic Discharge Immunity Test*.
31. A. Feller, H. R. Kaupp, and J. J. Digiacoma, Eds., "Crosstalk and and reflections in high-speed digital systems," Fall Joint Computer Conference, 1965. [CrossRef]
32. N. Mora, F. Vega, G. Lugrin, F. Rachidi, and M. Rubinstein, *System Design and Assessment Notes*, Vol. 41, 2014.
33. *IEC 61000-4-25 (2012), Electromagnetic Compatibility (EMC) Part 4–25: Testing and Measurement Techniques – HEMP Immunity Test Methods for Equipment and Systems*.
34. *HVDA55x-Q1 5-V CAN Transceiver with I/O Level Adapting and Low-Power-Mode Supply Optimization, Datasheet*. Texas Instruments Incorporated, 2016.

Georgiy Y. Kim was born in Tekeli, Kazakhstan, in 1996. He received M.Sc. degrees in Infocommunication Technologies and Communication Systems from TUSUR, Tomsk, Russia, in 2020. Currently, he is a Ph.D. student in Electromagnetic Compatibility of Radioelectronic Devices at TUSUR. He is the author and coauthor of 11 scientific papers.

Alexander V. Nosov was born in Semipalatinsk, Kazakhstan, in 1994. He received a bachelor's degree, master's degree, and Ph.D. degree in radio engineering from Tomsk State University of Control Systems and Radioelectronics (TUSUR), Tomsk, Russia, in 2015, in 2017, and in 2018, accordingly. Currently, he is working as a senior researcher at TUSUR. He is the author and coauthor of 82 scientific papers.